JGR Atmospheres

Key Points:

- Latent heat source data derived from space borne radar observation are used to estimate convective gravity wave momentum flux globally
- Mean conditional MF is generally larger over land than over ocean, mainly due to the larger latent heating rates
- There are still large differences in the convective GW MF between TRMM and WACCM6, due to representation of convection in the model

Author Contributions:
Conceptualization: Joan Alexander, Jadwiga Richter
Data curation: Chuntao Liu, Joan Alexander
Formal analysis: Chuntao Liu
Funding acquisition: Joan Alexander
Investigation: Chuntao Liu, Julio Bacmeister
Methodology: Chuntao Liu, Joan Alexander
Project Administration: Joan Alexander
Resources: Chuntao Liu
Software: Chuntao Liu, Joan Alexander
Validation: Chuntao Liu, Jadwiga Richter, Julio Bacmeister
Visualization: Chuntao Liu
Writing – original draft: Chuntao Liu

Using TRMM Latent Heat as a Source to Estimate Convection Induced Gravity Wave Momentum Flux in the Lower Stratosphere

Chuntao Liu[1] , **Joan Alexander[2]** , **Jadwiga Richter[3]** , and **Julio Bacmeister[3]**

[1]Department of Physical and Environmental Sciences, Texas A&M University – Corpus Christi, Corpus Christi, TX, USA, [2]NorthWest Research Associate, Boulder Office, Boulder, CO, USA, [3]National Center for Atmospheric Research, Boulder, CO, USA

Abstract Due to a lack of observations, it is a big challenge to quantify the momentum flux transported from the troposphere into the lower stratosphere by gravity waves generated by convection. This limits our understanding of the dynamics of general circulation in the stratosphere and the realism of simulations of the Quasi Biennial Oscillation. In the past decade, some general circulation models have linked the momentum flux to the latent heating from subgrid scale convective precipitation with some success. However, there is still a large uncertainty in the sources of subgrid scale convection in these models. This study applies the links between the momentum flux and convective latent heating directly to the convective precipitation derived from 16 years of TRMM precipitation radar observations in the tropics and subtropics. The total and directional momentum flux at 100 hPa are derived at individual convective pixels by using the TRMM Spectrum Latent Heating product and large-scale wind profiles from the ERA-Interim dataset. For the first time, we are able to estimate the geographical distribution of momentum flux at 100 hPa in tropics and subtropics from the observed convective sources. The diurnal, seasonal, and interannual variations of the derived momentum flux are presented and discussed. These results could provide a reference to validate the dynamic coupling between the tropical troposphere and the stratosphere in the general circulation models.

1. Introduction

It is well known that convective cloud systems in tropics drive the global circulation through latent heat release (Emanuel et al., 1994; Houze, 1989; Schumacher et al., 2004). Gravity waves generated by latent heating in tropical convection play an important role in transporting momentum from the troposphere into the stratosphere and may modulate the middle atmospheric circulation (Alexander et al., 2000; Collimore et al., 2003). The Quasi-Biennial Oscillation (QBO) of equatorial zonal winds with a period of ∼28 months is a prominent dynamical phenomenon in the equatorial stratosphere (Baldwin et al., 2001). To explicitly realize the QBO in the general circulation simulations, momentum flux (MF) from the troposphere into the stratosphere introduced by convection-induced gravity waves must be parameterized in the general circulation models (GCMs) (Beres et al., 2005; Bushell et al., 2015; Butchart et al., 2018; Chun & Baik, 2002; Giorgetta et al., 2006; Kim et al., 2013). However, most convective clouds have a spatial scale around a few kilometers. They cannot be explicitly resolved by the limited grid spacing around 100 km in general circulation models. Therefore, various cumulus parameterization schemes have been implemented in numerical models since the 1960s (Arakawa, 2004). Although there have been progressive developments in cumulus parameterization schemes in the past half century, there remain challenges to estimate realistic subgrid-scale latent heating and precipitation from convective clouds by various cumulus parameterization schemes (e.g., Arakawa, 2004; Kwon & Hong, 2017). Therefore, to diagnose and validate the parameterization of the MF from convective gravity wave sources in GCMs, two major uncertainty sources have to be dealt with. One source is from the subgrid-scale convective sources in GCMs. Another source is from imperfect assumptions in the parameterization schemes generating gravity wave MF and its spectrum from the estimated gravity wave sources. In this study, a method to estimate MF from observation-based convective gravity wave sources is introduced so that the uncertainty from convective sources can be largely mitigated.

It is clear that only satellites can provide observations to describe the convective gravity wave sources with a global coverage. Infrared and passive microwave observations from satellites have been used to provide a global view of clouds and precipitation for a long time (Huffman et al., 2001; Rossow & Schiffer, 1999). After the

launch of the first spaceborne precipitation radar onboard the Tropical Rainfall Measuring Mission (TRMM, Kummerow et al., 1998) in late 1997, the global convection in tropics and subtropics has been examined with unprecedented detail. Specifically, they have been analyzed in their intensity (Zipser et al., 2006), vertical structure (Houze et al., 2015), latent heat release (Shige et al., 2004; Tao et al., 2006), and variations at different time scales (e.g. Nesbitt & Zipser, 2003; Liu et al., 2019). During 16+ years of operation from December 1997 to September 2014, the TRMM precipitation radar has collected a significant number of observations and derived characteristics of precipitation and convection within 36°S–36°N. The instantaneous measurements provide the best available estimates of sources of convective gravity waves.

In this study, we have designed a method to apply a physically-based convective gravity wave source parameterization scheme (Beres et al., 2004, 2005) from the Whole Atmosphere Community Climate Model Version 6 (WACCM6, Gettelman et al., 2019) to the TRMM products. Using this method, we are able to estimate the MF within the limits of the gravity wave parameterization from TRMM convective gravity wave sources in tropics and subtropics (Alexander et al., 2021) and attempt to address the following questions:

1. What is the geographical distribution of convective gravity wave sources? How much MF is contributed by convection over different regions in the tropics and subtropics?
2. What are the different contributions of shallow or deep convection to the total MF in the lower stratosphere in tropics and subtropics? How are properties of convection related to their MF contributions?
3. How do directional components of MF in the lower stratosphere vary over different regions and different time scales, such as diurnally, seasonally, and interannually?
4. What are the uncertainties in the convective gravity wave sources from observations and parameterization schemes in GCMs?

In the following sections, the physical basis of the MF parameterization, data and methodology used in this study are introduced first in Section 2. Then, the global MF near the tropopause in tropics and subtropics are estimated by applying the WACCM6 parameterization scheme to 16-year TRMM convective sources. Spatial and temporal variations of the MF are presented in Section 3. The uncertainty in these analyses are discussed in Section 4, and the major findings are summarized in Section 5.

2. Data and Methodology

In WACCM6, the parameterization scheme of MF from convective gravity wave sources follows the line of study by Beres et al., (2004, 2005) and Richter et al., (2010). This scheme utilizes the subgrid scale Latent Heating rates (LH) in the model to estimate MF. However, the cloud LH is difficult to measure in reality. Therefore, assumptions of LH properties in convection and their large-scale environments have to be made in order to apply the parameterization scheme to the TRMM datasets.

2.1. Estimation of Momentum Flux Using a Simple Lookup Table Approach

As described in Beres et al. (2005), the wave source spectrum can be calculated at the top of the heating region of convection as a two-dimensional MF spectrum in frequency and wavenumber. In practice, the calculation of momentum flux can be simplified by introducing a predefined lookup table in Equation 1.

$$F(h, v_r, v_p, Q) = F_{LT}(h, v_r, v_p) \ Q^2 \tag{1}$$

where h is LH depth, v_r is relative mean wind from the layer of LH to 700 hPa, v_p is phase speed, Q is the maximum latent heating rate, and $F_{LT}(h, v_r, v_p)$ is the predefined lookup table by integrating the wave spectra. Here the mean wind of heating layer is calculated by averaging the wind with positive LH. The steering wind at 700 hPa is assumed to describe the motion of convection. vr is projected wind vector from heating layer to the convection motion.

To build the lookup table $F_{LT}(h, v_r, v_p)$, a few key parameters are needed, including heating frequency distribution, horizontal scale, depth of the heating, and the mean wind vector in the heating region. In WACCM6, the horizontal scales of convective cells within the convective region is assumed to be 3 km in diameter. A red-noise frequency distribution for wave periods between 10 and 120 min is also assumed. The lookup table is created as
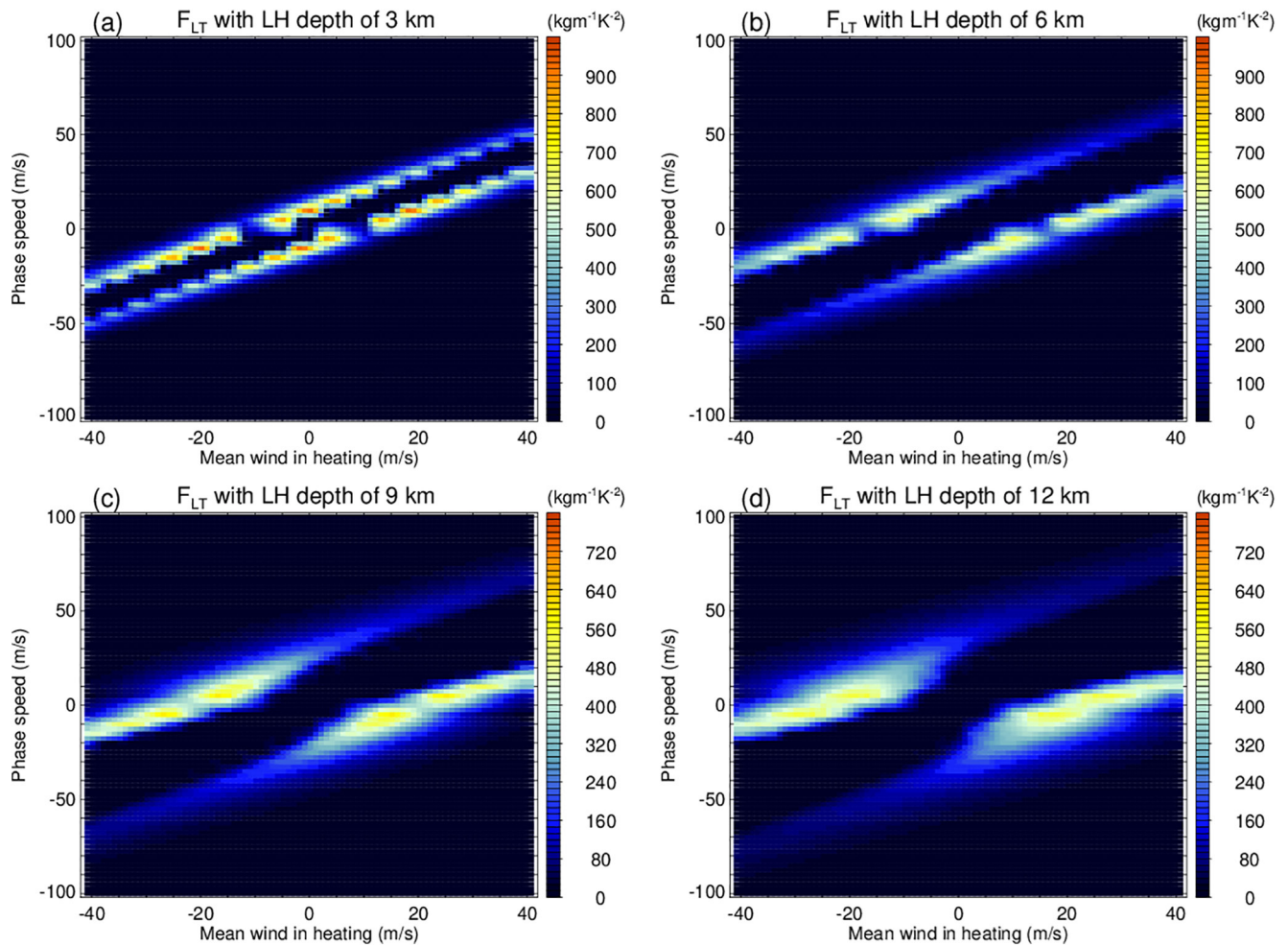
Figure 1. An example of the lookup table for F_{LT} in Equation 1 showing the momentum flux as function of intrinsic phase speed and mean relative wind in convective cells with four different latent heating depths.

discrete set of phase speeds ranging from ± 100 ms^{-1} with 2.5 ms^{-1} intervals, mean relative LH layer wind with values ranging from ± 40 ms^{-1} with 1 ms^{-1} intervals, and heating depth with values ranging from 1–20 km with 1 km intervals. An example of the lookup table F_{LT} in Equation 1 is shown in Figure 1. Compared to the deep heating profiles (Figure 1d), shallower convective heating depth (Figures 1a–1c) would have larger wave MF at lower phase speed. As expected, mean relative wind would determine the directional variation in the momentum flux. This lookup table is implemented in the current WACCM6 to parameterize the MF by using model derived latent heating profiles after assuming a sub-grid areal fraction of convection.

2.2. TRMM Convective Latent Heat and ERA-Interim Large-Scale Wind Fields

TRMM was launched in 1997 with the first space born Precipitation Radar (PR) onboard (Kummerow et al., 1998). Before the end of mission in 2014, TRMM PR had collected the radar reflectivity at a resolution with 4.5 km in horizontal and 250 m in vertical describing vertical structure of precipitation in detail. With about 17 years of observation from non-sun synchronous orbit between 36°S–36°N, it provided a robust measurement of properties of convection and precipitation and their diurnal, seasonal and interannual variations in tropics and subtropics (e.g., Houze et al., 2015; Liu, 2011; Liu and Zipser, 2008). To provide the latent heating in observed convective cells, the version 7 pixel-level TRMM Spectral Latent Heating (SLH) dataset during 1998–2013 is used. In this product, the latent heating profile is derived by using the convective precipitation rates (Iguchi et al., 2000, 2009) and radar echo top height. Here precipitation rate is used to define the heating strength, and the echo top height is used to constrain the heating depth. Based on the precipitation types, different lookup tables are applied to the

pixels with convective and stratiform precipitation separately. The convective and stratiform precipitation types are differentiated by examining the horizontal and vertical gradients of radar reflectivity as well as the presence of the reflectivity bright band (Awaka et al., 1998, 2009). The lookup tables relating precipitation rates and echo top heights to latent heating profiles are built based on the cloud resolving model simulations of a few field campaigns. Details of the SLH retrieval algorithm are described in Shige et al., (2004, 2009). As a hybrid approach of using simulated LH vertical structure constrained by observations, this product has been used to derive the global LH vertical structures statistically (Liu et al., 2015; Takayabu et al., 2010; Tao et al., 2016). However, at each individual pixel level, there could still be a large uncertainty in the instantaneous LH profile due to the assumptions made in the retrieval algorithm. We will revisit the uncertainties in the LH retrievals in Section 4.

In this study, the SLH latent heating profiles with 1 km vertical resolution at pixels with convective precipitation during 1998–2013 are used. At each pixel with convective precipitation, the maximum latent heating values (Q) are calculated from the LH profiles. To determine the V_r in Equation 1, large-scale wind vector profiles are temporally interpolated from 6 hourly wind field in ERA-Interim reanalysis dataset (Dee et al., 2011) from the nearest $0.75° \times 0.75°$ grid. Then the mean wind vectors in the layer with positive LH values, at 100 hPa, and 700 hPa are saved for each pixel. To apply the lookup table $F_{LT}(h, v_r, v_p)$ in Equation 1 to the TRMM convective pixels, the difference in the assumption of convection size has to be addressed. TRMM PR have footprint size about 4.5 km, which is larger than the 3 km size assumed in the lookup table from WACCM. Therefore, the difference in area factor 2.2 has been used when applying the lookup table.

The geographical distribution of the population of more than 3×10^8 TRMM SLH profiles with convective precipitation over the course of 16 years is shown in Figure 2a. A large number of profile samples is adequate to generate robust statistics on $1° \times 1°$ grids in tropics and subtropics. Note that there are more profile samples near 32°N/S latitudes due to the TRMM orbital inclination. This sample bias is removed from all the convection and gravity wave statistics in this study after normalizing by the total sampled pixels or by averaging. The geographical distributions of mean LH depth, and maximum LH in the profile on $1° \times 1°$ grids are shown in Figures 2b and 2c. It is well known that convection over land tends to be stronger than over ocean (e.g., Zipser et al., 2006). There are numerous isolated shallow convective clouds over ocean (Liu & Zipser, 2009; Schumacher & Houze, 2003), whereas shallow convection can only be frequently found in specific regions over land, such as the Amazon and maritime continents. Most convection over tropical and subtropical land reach above the freezing level and have ice hydrometers. In general, this leads to a deeper convective heating layer and a stronger heating over land than over ocean, especially over the "hotspot" regions with the most intense convection, that is, central Africa, Southeast United States, Argentina etc. (Figures 2b and 2c).

The wind field plays a significant role in translating the convective latent heating to the gravity wave MF into the lower stratosphere. In the Inter-Tropical-Convergence-Zone (ITCZ), easterly wind is dominant in the lower troposphere, except over the north Indian Ocean (Figures 2b and 2d). At mid latitude, westerly wind is dominant. In addition to the regions with strong meridional trade winds, the 700 hPa wind determines the directional components of the total MF.

3. Results

After applying the MF lookup table to TRMM convective latent heating properties and ERA-Interim wind vectors, convective gravity wave MF at different phase speeds in four different directions at 100 hPa are derived at more than 3×10^8 convective pixels from 1998–2013.

3.1. Geographical Distribution of Convective Gravity Wave MF

The geographical distribution of mean MF at 100 hPa on $1° \times 1°$ grids are summarized in Figure 3. First, the total amount of absolute MF is integrated from full phase speed spectra at four directions on each $1° \times 1°$ grid. The conditional mean MF (Figure 3b) is calculated by dividing the total number of convective samples at each grid. The unconditional mean MF (Figure 3a) is calculated by dividing the total number of Ku radar pixel samples at each grid, including samples of non-precipitating pixels and those with non-convective precipitation. The distribution of the annual unconditional MF is close to the distribution of total annual convective precipitation in the literature (e.g., Houze et al., 2015; Schumacher & Houze, 2003), and similar to the map of total convective pixels in Figure 2a. There is a larger MF in the ITCZ and the South Pacific Convergence Zone (SPCZ) as well as
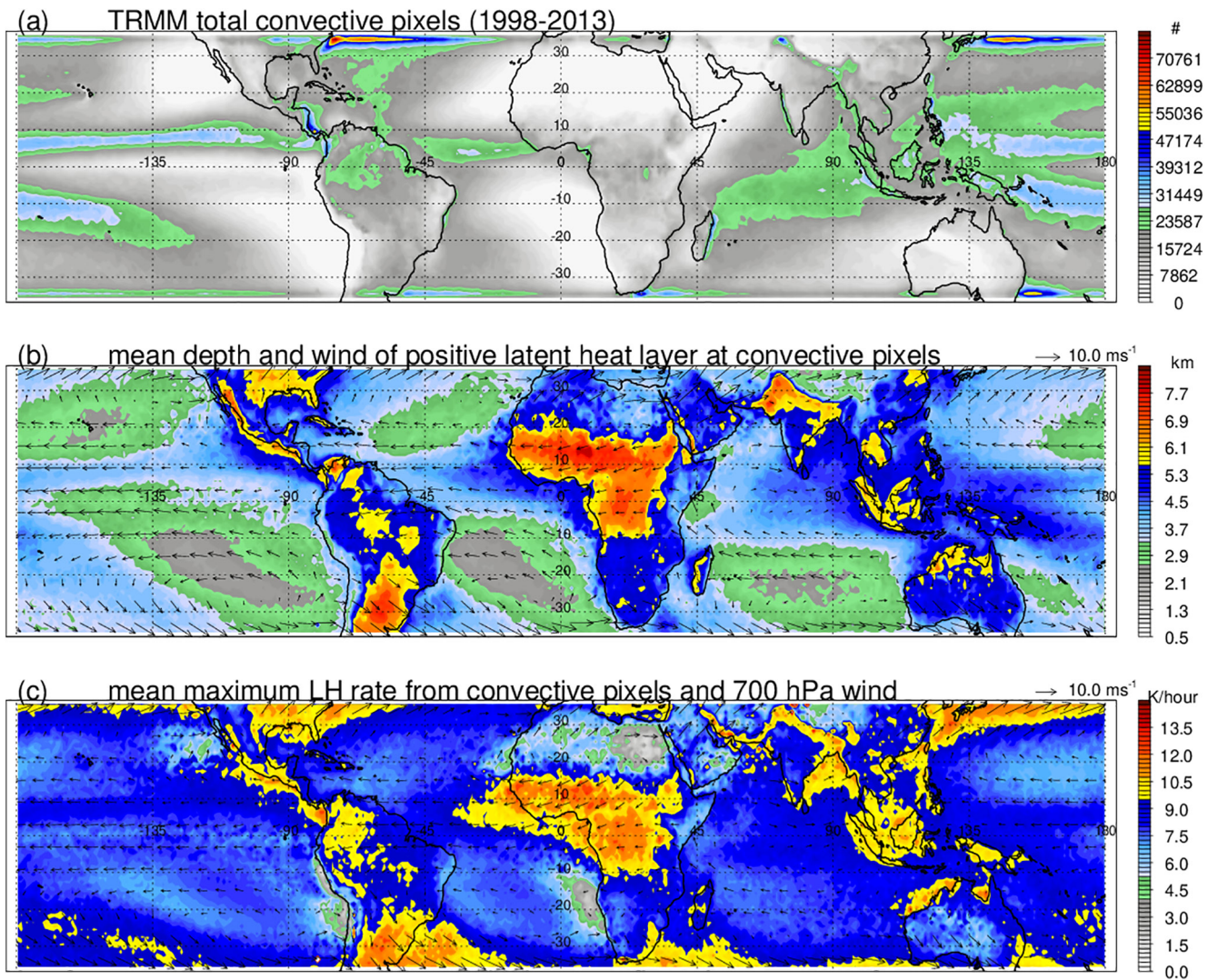
Figure 2. (a) geographical distribution of numbers of pixels on 1° × 1° grids with convective rainfall from tropical rainfall measuring mission (TRMM) during 1998–2013; Note that there are many fewer convective precipitation pixels over Northeast Australia due to no radar observations being collected over the region by TRMM satellite after a short time period of the mission. (b) mean depths of positive TRMM SLH latent heating at convective pixels. The mean wind vectors in the positive latent heat layer from ERA-Interim are overlaid; (c) mean maximum latent heating rate at convective pixels; mean 700 hPa wind vectors at these convective pixels are overlaid.

over a few warm ocean currents, e.g. the Gulf Stream in the west edge of North Atlantic and the Kurishio current in the west edge of the North Pacific. The distribution of conditional MF in Figure 3b is close to the distribution of mean maximum latent heating rate in Figure 2c. Mean conditional MF is generally larger over land, where the maximum latent heating is also larger, than it is over ocean.

3.2. Directional Convective Gravity Wave MF

The geographical distribution of components of unconditional MF at 100 hPa in four cardinal directions are shown in Figure 4. In the tropics, the eastward MF has the largest magnitude. This is corresponding to the prevalent heating layer easterly wind environment of the tropics (Figure 2b). Figure 1 showed that for deeper convective cells, momentum fluxes tend to be enhanced in the direction opposite to the flow. In the subtropics, westward MF is stronger (Figure 4b), corresponding to the dominant westerly wind environment at these latitudes. The meridional MFs at 100 hPa have relatively lower magnitudes compared to the east and westward MFs, which is associated with more frequent occurrences of zonally directed 700 hPa winds. In the tropics, a larger total
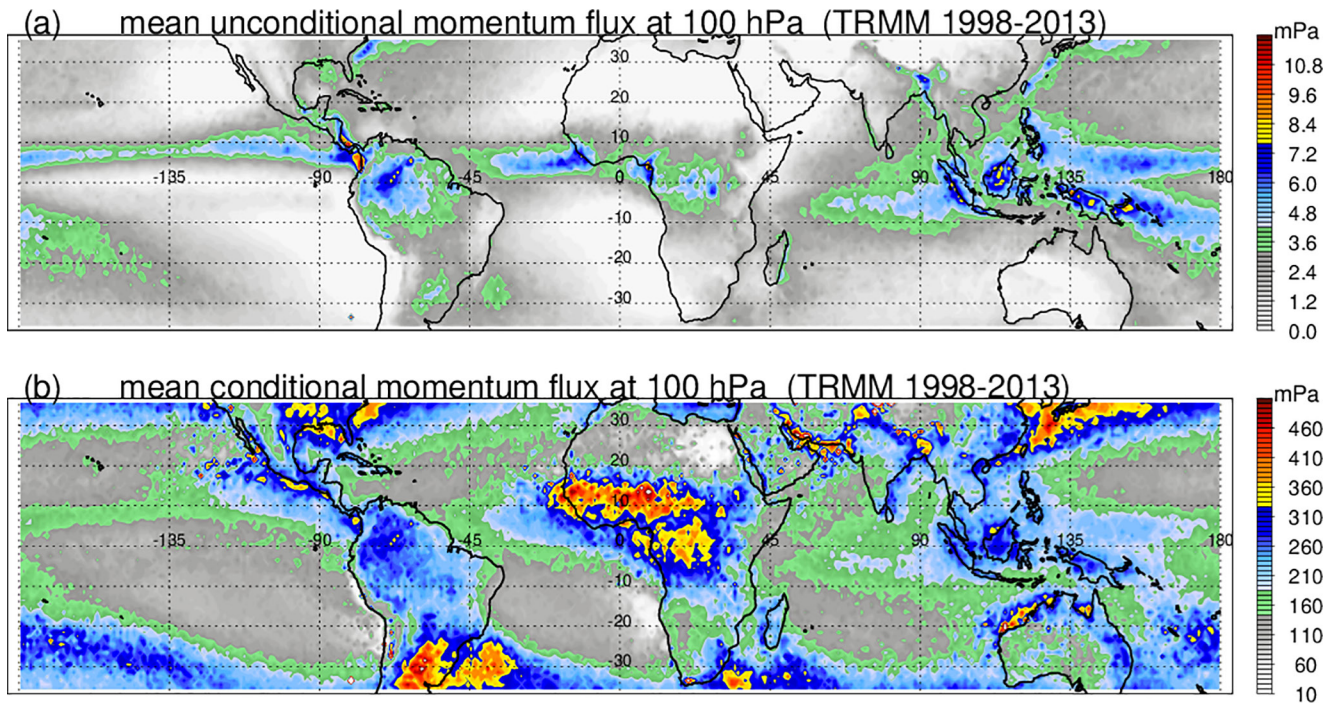
Figure 3. Geographical distribution of mean unconditional (a) and conditional (b) momentum flux at 100 hPa from 1998–2013.

meridional MF is found over the Maritime continents and Panama area. This is due to the combination of frequent relatively intense convection (Figure 2c) as well as the meridional flow steered by land and ocean interaction over these regions (Figure 2b). In the subtropics, larger meridional MF are found over the regions with warm ocean currents, for example, southward over the Gulf Stream and Kuroshio current (Figure 4d), and are populated with low level jets, e.g. over the plains east of the Rockies and Andes mountains. Both the main meridional flow and convection are stronger over these areas than over other places in spring and summer.

The geographical distribution of mean directional MF per convective cell (conditional MF) is shown in Figure 5. In the tropics, the intense convection in central Africa and Sahel is the most efficient at generating eastward MF at 100 hPa due to the large latent heating rate (Figures 2c, 3b and 5a, 5b). In the subtropics, intense convection occurs over warm currents and down slopes of major mountains where larger conditional westward MFs are found, including the southeastern US, Argentina, and the south slope of the Himalayas. Although the SPCZ has a large total MF (Figures 3a and 4), a larger mean westward and northward conditional MF is found south of the main SPCZ region (Figures 3b and 5). This is consistent with a relatively stronger convective heating (Figure 2c) and shallower heating depth (Figure 2b) over this region than over the main SPCZ region.

The geographical distributions of the total zonal (eastward-westward) and meridional (northward-southward) MF are shown in Figure 6. The zonal MF transport into the stratosphere is important in forcing the QBO in the tropics. It is clear that eastward MF dominates over the tropics in the 16-year mean (Figure 6a), with the exception of a small area of larger westward MF over the north Indian Ocean. The tropical eastward MF is on average about 20% larger than the westward MF. Model studies suggest that about half of the total forcing of the eastward QBO phase is by planetary scale Kelvin waves, with the other half of the forcing by gravity waves, while the forcing of the westward QBO phase is dominated by gravity waves. So the east-west asymmetry in the MF in Figure 6a appears to have the wrong sign. As pointed out in Alexander et al., (2021), other gravity wave components are probably needed to compensate for the eastward dominance in the current calculation, such as the stationary wave MF. Regarding the meridional MF, subtropical MF mostly points toward the equator. In the tropics, northward MF is more prevalent, especially over the Sahel and India, which is driven by the summer monsoon circulations (Hahn & Manabe, 1975; Parker et al., 2005).

We further examine tropical convection of various depths and their contributions to the total MF in Figure 7. In the tropics (20°S–20°N), more convective cells (79.3%) occur over ocean than over land mainly due to the
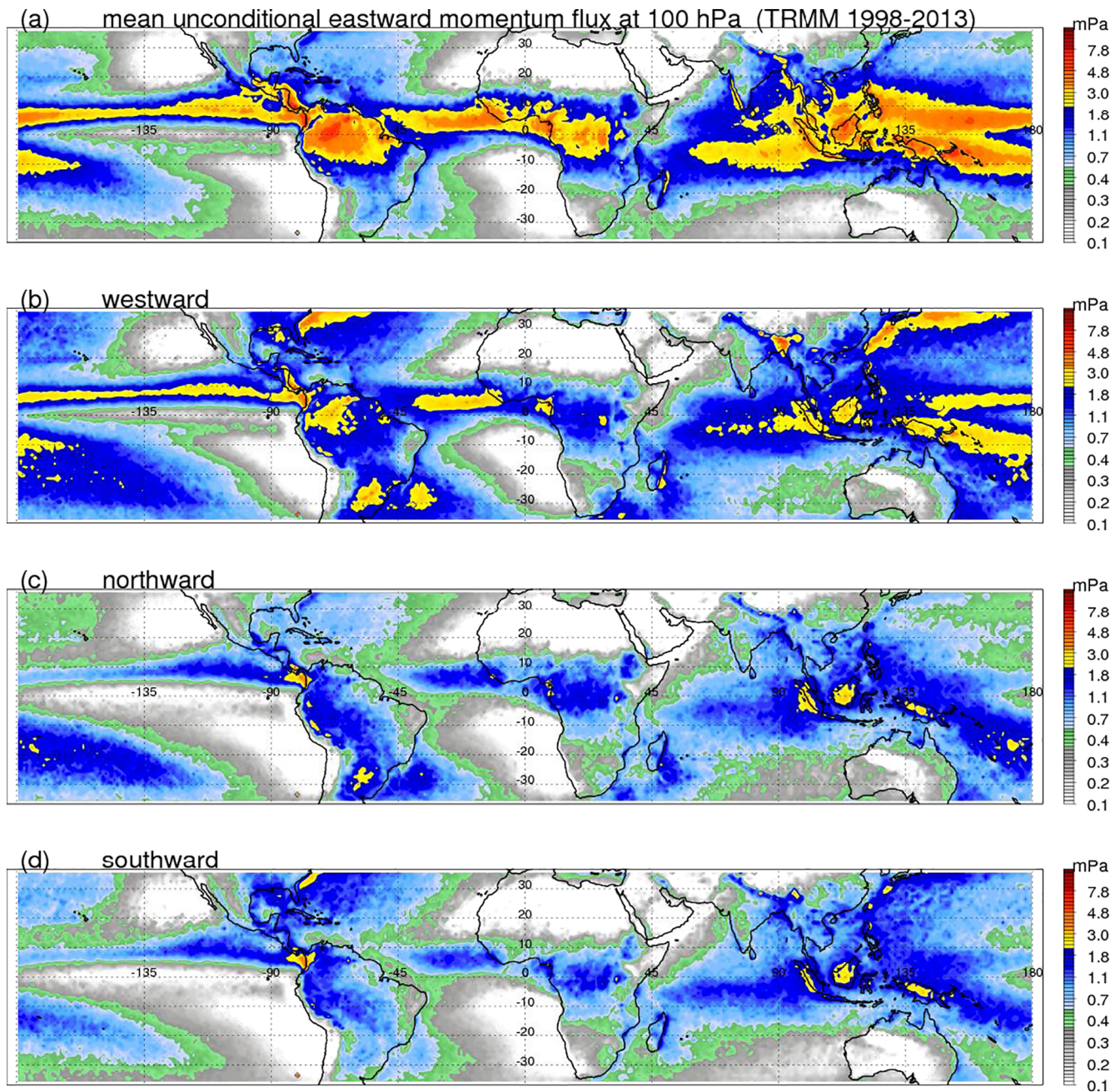
Figure 4. Geographical distribution of mean unconditional momentum flux at 100 hPa in (a) eastward; (b) westward; (c) northward; (d) southward directions.

71% ocean coverage of the globe. Over tropical ocean, shallow convection with echo top height below 4.5 km, a height around 0°C, is more frequent than the convection with ice that is indicated by the echo top height above the freezing level (Figure 7a). Over land, more convective cells include ice processes. In general, convection that develops deeper and lifts hydrometeors above the freezing level are more intense and have relatively larger latent heating rate and higher surface precipitation rate than shallow convection. Though less frequent than shallow convection, convection with echo top height above freezing level around 6–8 km contribute to a larger proportion of the total MF in the lower stratosphere (Figure 7b). There are numerous samples of shallow convection over ocean. They have a significant contribution to the westward MF, which could be very important for understanding how waves drive QBO. Though there are more deep convective pixels with radar echo top reaching above 12 km over land than over ocean, they do not contribute a dominant portion of the net east and west MF. This
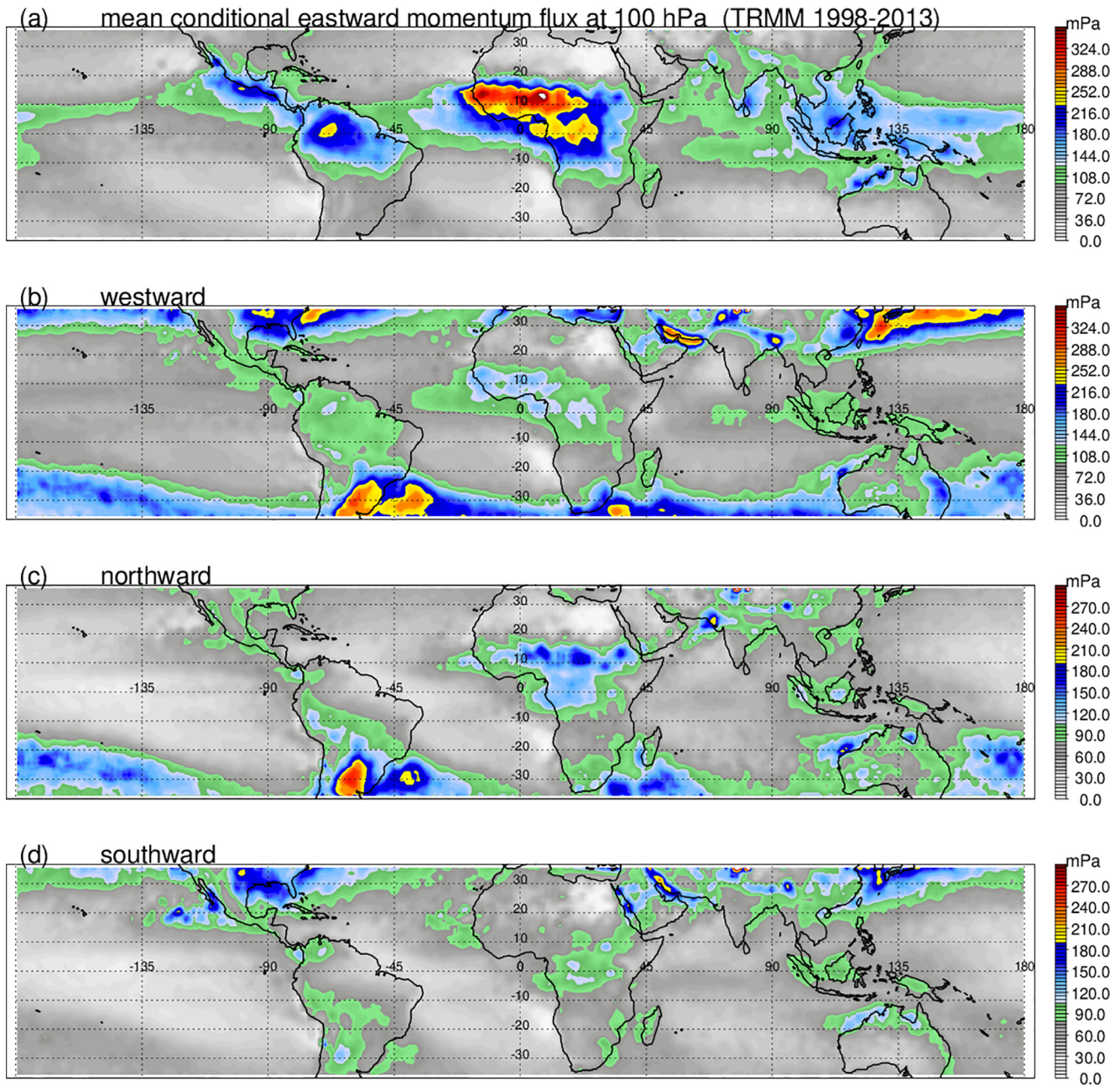
Figure 5. Geographical distribution of mean conditional momentum flux at 100 hPa in (a) eastward; (b) westward; (c) northward; (d) southward directions.

is somewhat surprising since the deep convection over land is associated with stronger gravity waves that are detectable in the mid-upper stratosphere from satellites (e.g., Ern et al., 2018; Hoffmann et al., 2013; Hoffmann & Alexander, 2009). Here the MF shown in Figure 7 are analyzed at 100 hPa. This may be due in part to satellite observational filters and limited local time coverage, but also shallower clouds may be associated with slower phase speed waves that more often dissipate below the satellite observation levels.

3.3. Diurnal Variation

It is well known that convection has a distinct diurnal variation over land and a weak variation over ocean (Gray & Jacobson, 1977; Hall & Vonder Haar, 1999; Liu & Zipser, 2009; Nesbitt & Zipser, 2003). Consequently, diurnal variation of the convective gravity wave MF is anticipated. However, the diurnal variations of the eastward and
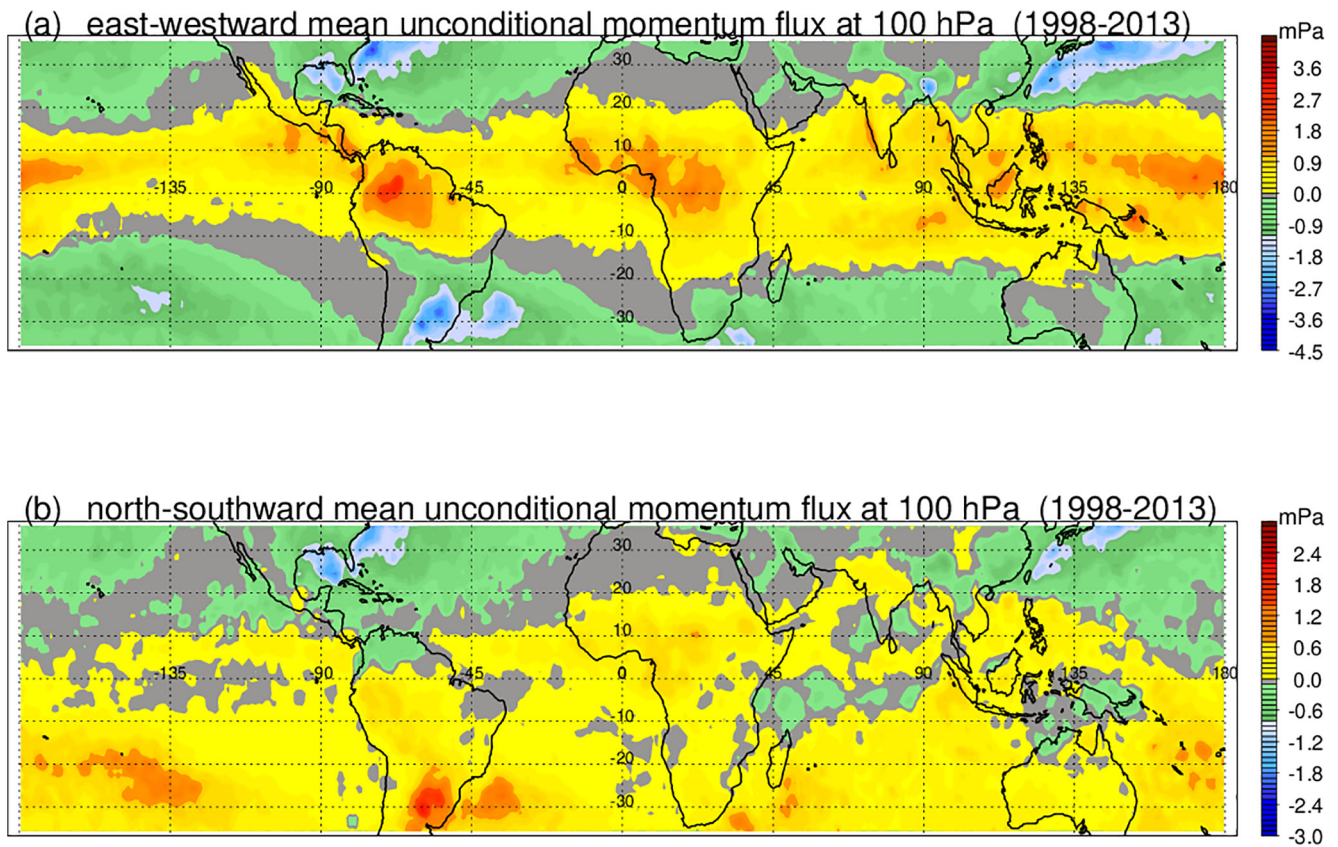
Figure 6. Geographical distribution of mean net unconditional momentum flux at 100 hPa in east-west direction (a) and north-south direction (b).

westward MF could be quite different from the convective latent heating. This is because wind vectors change diurnally over some specific regions, especially near mountains (e.g. Banta et al., 2004) and coasts (e.g. Miller et al., 2003). As shown in Figure 8, an obvious peak of high MF in the early afternoon around 1,500 LT is found over tropical land, which corresponds to the numerous isolated and early stages of organized convection over land. Note that this peak is prior to the late afternoon peaks around 1,700 LT in cold clouds, when organized convective systems mature (Liu & Zipser, 2008). In the tropics as a whole, the diurnal variation of the total eastward and westward MF is relatively weak due to the dominance of the oceanic convection, which varies only slightly at different times of the day. Though only covering 29% of the area in the tropics, land has a total amount MF that is comparable to MF of the ocean in 1,400–1,700 LT. Therefore, the late afternoon peak at 1,400–1,500 LT appears in the diurnal variation of total MF in tropics in Figure 8a.

3.4. Seasonal Variation

In order to compare to the previous study of Richter et al., (2010) and examine differences by using the observed convective sources and reanalysis wind fields, the mean unconditional MFs from 16-year TRMM convective pixels are calculated as a function of month and latitude. This is shown in Figure 9. The pattern of MF seasonal-latitudinal variation is close to the result from WACCM3.5 (i.e., Figure 2 of Richter et al., 2010) with a few significant differences. First, the magnitude of the MF is about ~50% weaker than the result of WACCM3.5. Compared to Richter et al., (2010), results from TRMM show earlier seasonal peaks in all directions, for example, TRMM eastward MF peaks in June vs. WACCM in July. Similar patterns are observed from TRMM vs. WACCM, respectively: westward in May–June vs. June–July, northward in August–September vs. September–October, southward in August vs. September. Results using TRMM do not show a clear strip of MF south of equator as WACCM does, which is likely from the known issue of an exaggerated secondary ITCZ in general circulation models (Lin, 2007).
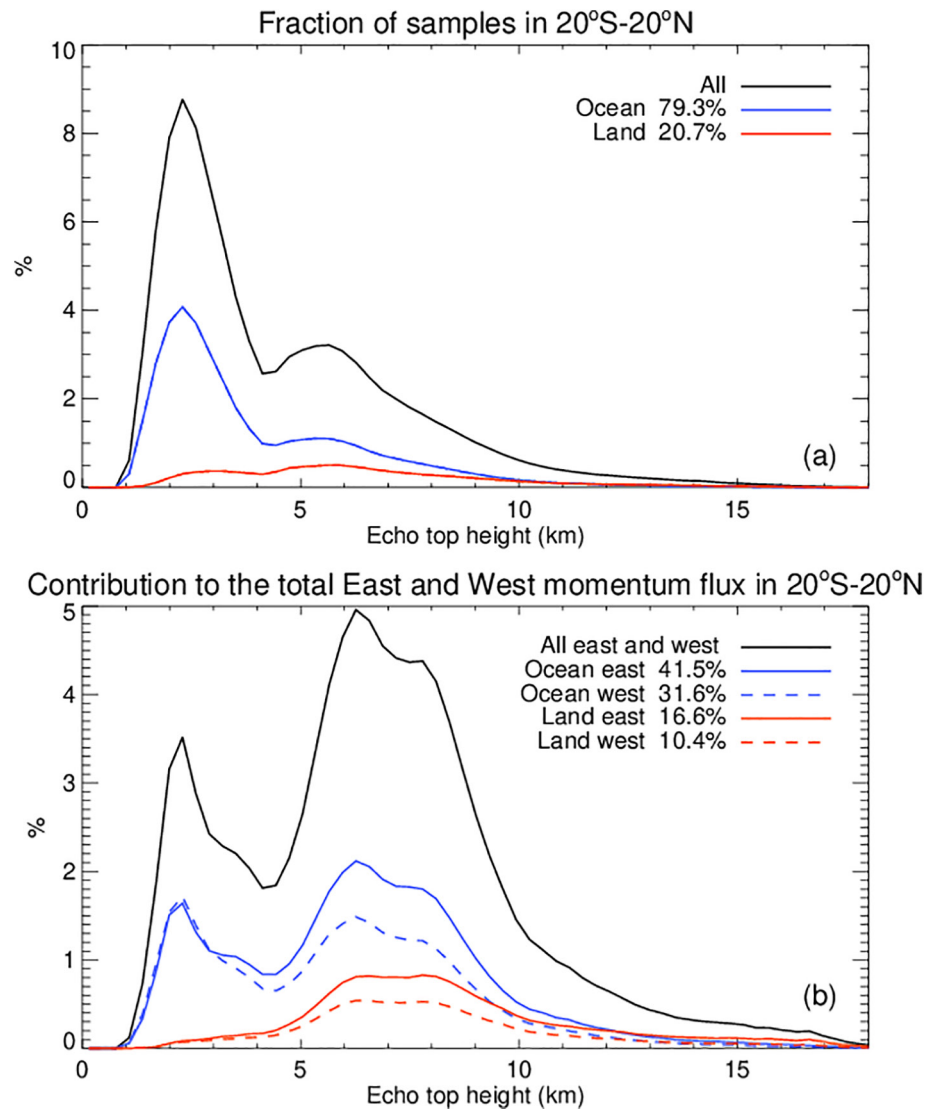
Figure 7. (a) Histograms of tropical rainfall measuring mission (TRMM) convective pixels in 2010 as function of radar echo top height over tropical land and ocean and their mean maximum latent heating rate (dashed lines); (b) contribution of east-west momentum flux at 100 hPa from convection of different depth over tropical land and ocean.

It is important to understand the regional contributions of eastward and westward MFs and their seasonal variations in the tropics. The mean unconditional MF as a function of month and longitude between 20°S–20°N is shown in Figure 10. In the tropics, large magnitudes of MF are contributed by convection over major continents, including over all seasons in the Americas (50°–100°W), March-May and September-November in central Africa (10°W–30°E), India and Bangladesh during summer monsoon (80°–100°E), Northern Australia and Maritime continent in December–February (110°–150°E), and June-October in the tropical West Pacific (140°–170°E). Among all these regions, it is interesting to see a weak contribution over Africa, where the most intense convection occurs frequently in all seasons, especially in transition seasons during north-south propagation of the ITCZ. Though eastward MF dominates over most regions and seasons, in the tropical central Pacific (180°–100°W), westward MF is greater in October–May (Figure 10c).

3.5. Interannual Variation

The QBO has been recognized as having links to the ENSO cycles (Gray et al., 1992). To interpret interannual variation in MF, the variation of zonal circulation in tropical troposphere could be crucial. Interannual variation
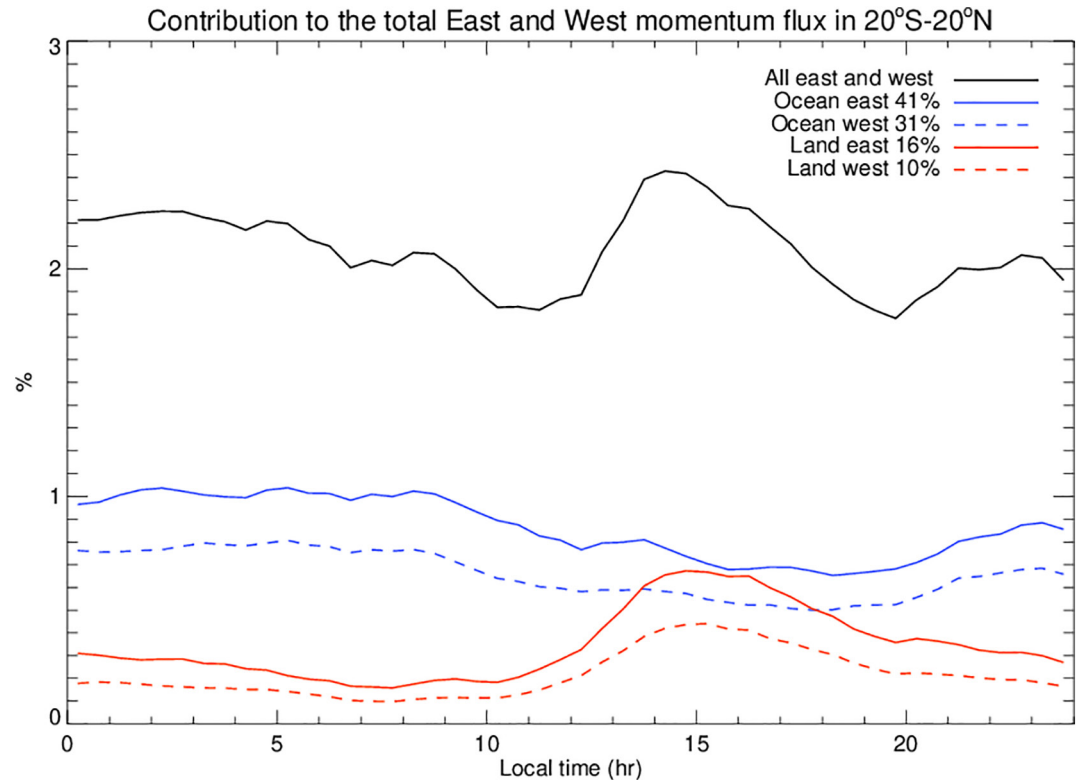
Figure 8. Diurnal variation of east and westward gravity wave momentum flux at 100 hPa from convection over tropical land and ocean. This figure is created by accumulating directional momentum flux (MFs) at convective pixels in 2010 in half local hour bins.

of zonal winds and convection may directly modulate the MF (Alexander et al., 2017). During the 16+ year TRMM era, there are several ENSO cycles that are closely tied to the strength of Walker circulation (Power & Smith, 2007), including strong ENSO cycles in 1998–1999 and 2010–2011 (Figures 11a). This provides enough samples to examine the general differences in convection and precipitation between two ENSO phases (e.g., Liu et al., 2019). Using the multi-variational ENSO index (Wolter & Timlin, 2011), we selected three Januarys with the highest positive and the lowest negative index values and repeated the process for February through December as shown in Figure 11. Then, the mean eastward and westward MF and their differences as a function of month and longitude are calculated from 36 months of data in two different ENSO phases. Compared to the westward MF, the eastward MF is stronger over maritime continents in the La Nina phase when a stronger Walker circulation is driven by the warmer west Pacific and relatively cold east Pacific. In consistence with literature, convection is more active over South America under La Nina. During the El Nino phase, westward MF is more comparable to the eastward MF, especially during January-April.

4. Uncertainties and Comparison to WACCM6

Using TRMM observations, we are able to estimate MF at 100 hPa in tropics and subtropics and examine the variation of MF at different time scales. However, there are many assumptions in the calculations that should be mitigated to understand the uncertainties in these results.

4.1. Uncertainties in the Implementation of Beres' Method

In this study, we used a lookup table created for the WACCM to estimate the MF. There are several assumptions built in this lookup table. First, the size of the convective cell is assumed to be 3 km. This is somewhat comparable to the TRMM PR footprint (~4.5 km), and it is taken into account by an area adjustment factor. However, the size of the updraft cores varies significantly from sub kilometer in single cells to 7–10 km in super cells
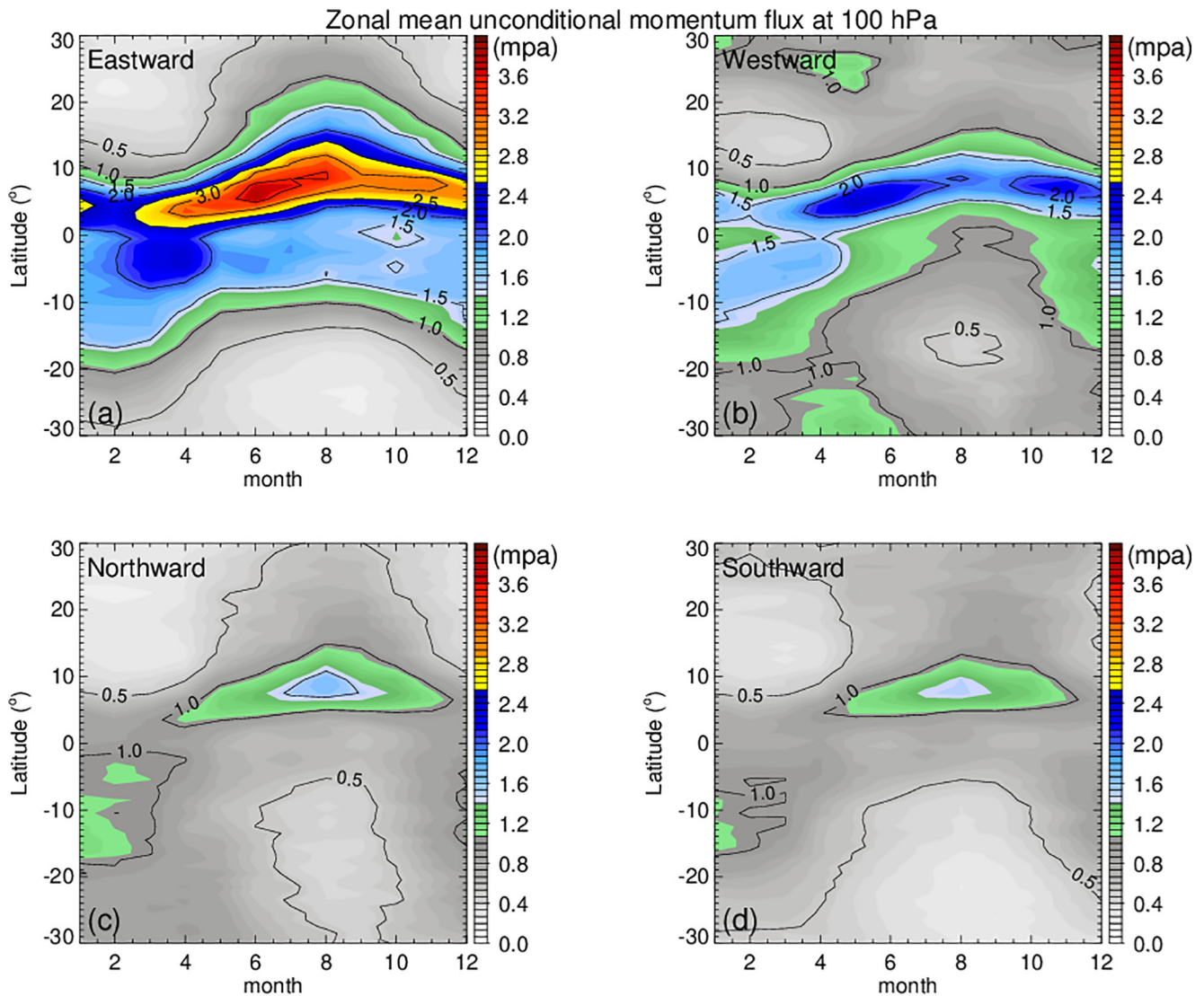
Figure 9. Gravity wave momentum flux at 100 hPa derived from applying the lookup table to TRMM LH as a function of time and latitude. (a) Eastward, (b) westward, (c) northward, and (d) southward momentum flux contributions. Contours are in equal intervals of 0.5 mPa.

(Giangrande et al., 2013; Heymsfield et al., 2010). It is questionable that a universal size of convection can represent the variation of convection and their intensity.

Westward MF is found relatively weaker than eastward MF in the current estimation from TRMM. Based on Figure 7b, the shallow convection over tropical ocean would contribute to a substantial westward MF. This may point to the key role of shallow convection. Note that TRMM PR can only detect radar reflectivity above 18 dBZ. It misses all of the cumulus clouds without precipitation size hydrometeors (Lebsock & L'Ecuyer, 2011). Because most of these cumulus clouds are shallow, they may have large MF contributions. This raises a question whether observations sensitive to small cloud droplets, such as from CloudSat, should be used to include weak cloud systems in the MF calculation. This makes it more difficult to understand the directional MF transport into the stratosphere necessary to interpret the QBO.

4.2. Uncertainties in the Convective Latent Heating Data

Only the TRMM PR pixels with convective type precipitation are used in this study. The algorithm to separate convective and stratiform precipitation types (Awaka et al., 1998; Awaka et al., 2009) relies on the detection of the
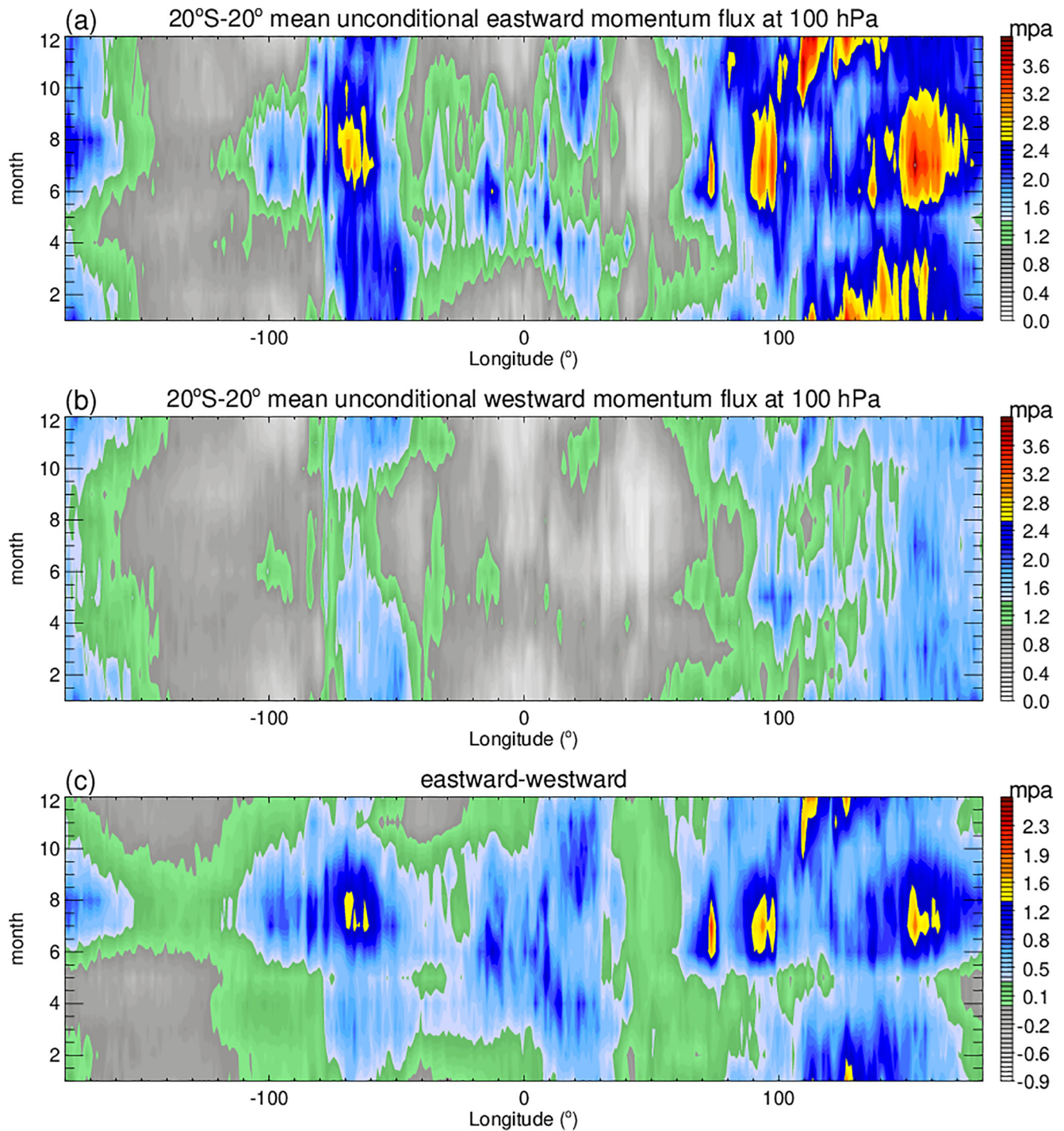
Figure 10. Gravity wave momentum flux at 100 hPa derived from TRMM LH as a function of time and longitude. (a) Eastward, (b) westward, (c) eastward-westward.

bright band from the horizontal and vertical gradients of radar reflectivity values. It is not always accurate over some specific regions (Funk and Schumacher 2013). However, the misclassification of convective precipitation should not be significant in this study at a global scale.

Because latent heat releases when hydrometeors form and grow, the radar observed hydrometeors with larger precipitation sizes must have a time lag from the heat release. Because of this time lag, the location of radar echo can be mismatched from when and where the latent heating occurs. The retrievals at each satellite pixel may not
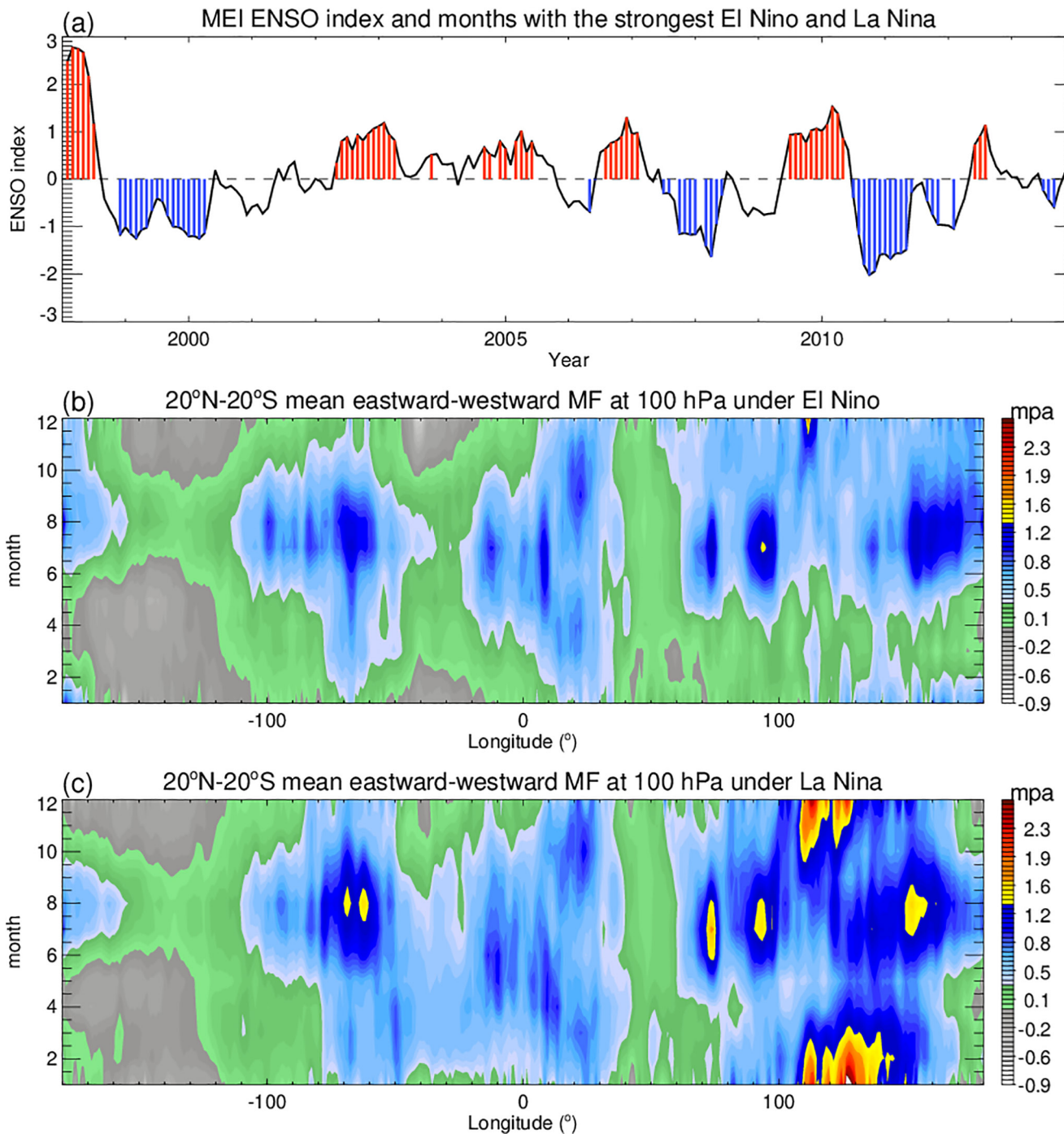
Figure 11. (a) multivariate ENSO index and 36 months with the strongest El Nino and La Nina indices during TRMM era; (b) eastward-westward momentum flux differences in tropics during El Nino; (c) same as (b) but for La Nina.

necessarily represent the true instantaneous latent heating rate. Especially, the heating rate in intense convection can be underestimated at pixels because most of the hydrometeors lifted by intense updrafts would fall at a different location. There is an inequality between the surface convective precipitation and latent heat release through the strong updraft cores at pixel level. This may lead to an underestimated MF from deep convection. Note that deep convection contributes more to the eastward MF (Figure 7b). If the contribution of MF from deep convection is enhanced, the eastward MF would be even stronger.

Table 1
Mean Unconditional Total and Directional MF Over Tropics (20°S–20°N) in 2010 Calculated From TRMM by Using 700 hPa, 850 hPa Steering Wind, and From WACCM6

MF at 100 hPa (mPa)	Total	Eastward	Westward	Northward	Southward
TRMM with 700 hPa steering wind	2.36	1.48	1.07	0.70	0.67
TRMM with 850 hPa steering wind	2.31	1.41	1.05	0.72	0.70
WACCM6	2.00	0.70	0.56	0.35	0.38

4.3. Uncertainties in the Wind Field

Wind field directly determines the direction of MF transport into the stratosphere. In this study, we interpolated 0.75°, 6 hourly ERA-Interim U and V components at pressure levels to the time and location of TRMM convective pixels to describe the wind field at 100 hPa, steering wind at 700 hPa, and mean wind through the heating depth. It is well known that wind shear at low levels plays an important role in the intense convection (Weisman & Klemp, 1982; Weisman & Rotunno, 2000). The moist transport by low-level jets of different depths is one key feature for intense convection over different hotspot regions around the world (Liu et al., 2020). A slight difference in the timing of convection and height of steering wind could lead to quite different MF directional components. This leads to a question of how accurately ERA-Interim large-scale circulation can represent the wind vectors associated with mesoscales. For example, to test the impact of the steering level wind, the MFs are calculated by using U and V at 850 hPa instead of 700 hPa in 2010. The result is shown in Table 1. Though the geographical patterns of directional MF are close to each other (Figure is not shown), the magnitudes of meridional MF components have slight increases if the wind at 850 hPa is used as the steering wind. Therefore, we have to be cautious of the uncertainty in directional MF that is quite sensitive to the accuracy of the wind fields.

4.4. Comparison to WACCM6

Keeping all above uncertainties in mind, the objective of this study is to build an observation-driven dataset to diagnose, validate, and understand the weaknesses of the parameterization of convective gravity wave momentum flux in GCMs. A comparison of the mean annual total MFs at 100 hPa in 2010 generated by WACCM6 and TRMM is shown in Figure 12. There are several obvious regional differences between WACCM6 and TRMM. Near Panama and Indonesia, WACCM6 have generated much larger MF than TRMM (Figure 12a). WACCM6 underestimates the MF over the central Amazon and central Africa, but overestimates the MF over the Brazilian high plains compared to what TRMM estimates. Sharing the same problem of exaggerated double ITCZ by GCMs (Lin, 2007; Zhang et al., 2019), WACCM6 generates a secondary ITCZ near the equator and a weaker ITCZ over the central and west Pacific (Figure 12a) than what TRMM suggests (Figure 12b). It is important to note that WACCM6 does not produce much MF in the subtropics due to tapering convective gravity waves to zeros by 30° latitude. Therefore, on average, WACCM6 has smaller MF transport in the tropics than what TRMM estimates (Table 1). Though there are many different ways to diagnose the differences between the WACCM6 and TRMM, the detailed comparisons between WACCM6 and TRMM calculations warrants a separate study.

5. Summary

After applying WACCM6 convective gravity wave MF parameterization to the TRMM observed 16-year convection sources, gravity wave momentum flux in the lower stratosphere is estimated globally over the tropics and the subtropics. The major findings include:

1. 16 years of TRMM observations describe the variations of convection in the tropics and the subtropics well. The latent heat retrievals from TRMM observations can be used to estimate the momentum transport into the lower stratosphere by gravity waves associated with convection. This could provide a tool to validate the parameterization of momentum transport by convection at different time scales.
2. Based on the current WACCM convective gravity wave parameterization, the magnitude of MF from convection is related to the depth and magnitude of latent heating rate, the wind vectors in the heating layer, and the horizontal motion of convection. Mean conditional MF is generally larger over land than over ocean, mainly due to the larger latent heating rates.
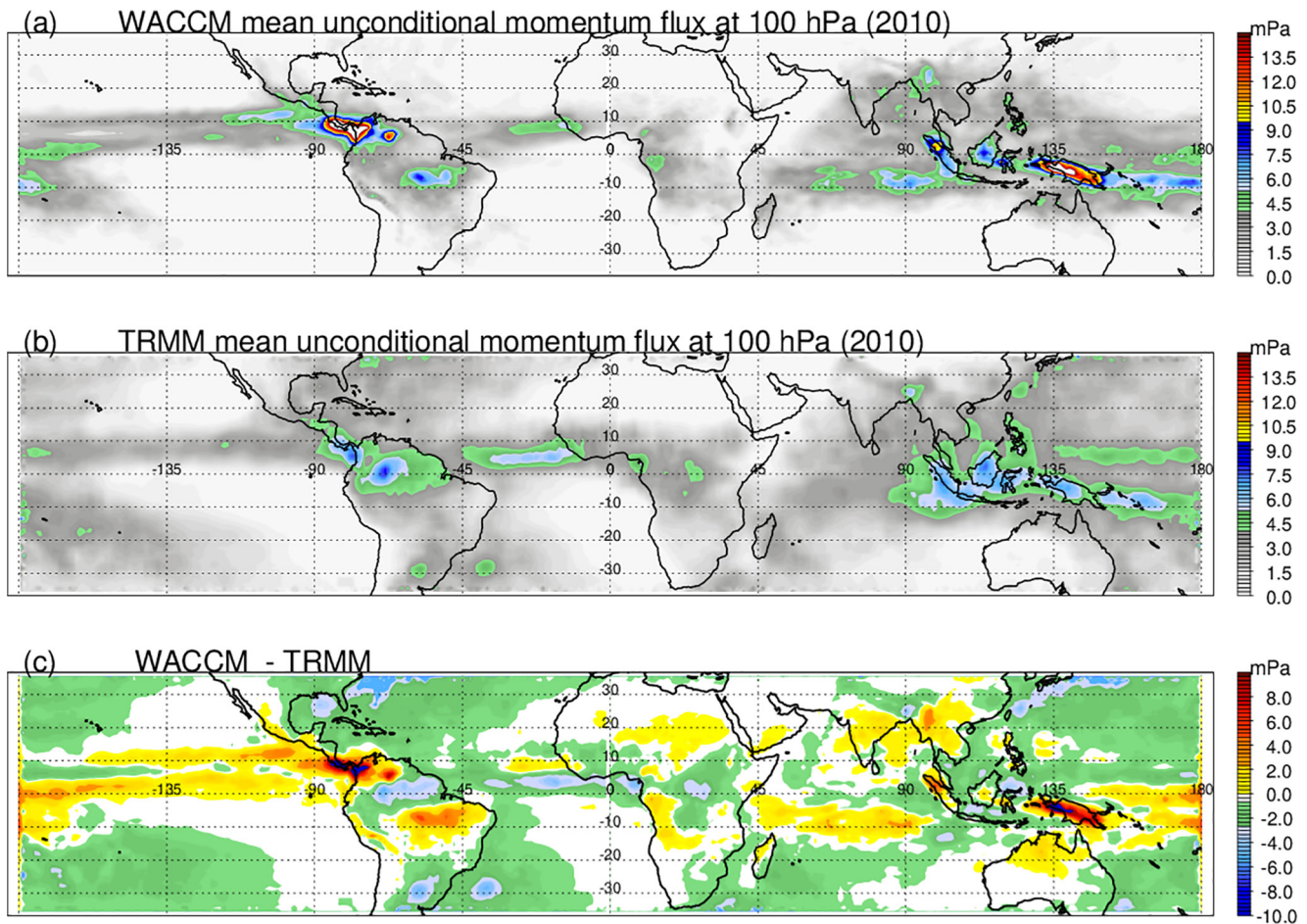
Figure 12. (a) mean unconditional WACCM GW total momentum flux at 100 hPa in 2010; (b) same as (a) but estimated from TRMM convective pixels from 2010; (c) the differences (a, b) between WACCM and TRMM total unconditional momentum flux.

3. There are still large differences in the convective gravity wave momentum flux between TRMM and WAC-CM6. In addition to the different latent heat rates along with the precipitation amount between the two, the differences in wind circulation around convection could be another factor.

4. Uncertainty of TRMM MF calculation may be from the assumptions in the model parameterization and the simplification of Equation 1, from inaccurate wind field due to coarse temporal and spatial resolution of reanalysis data, regional circulation errors associated with mismatch between reanalyzed precipitation and TRMM precipitation, and from TRMM LH retrievals. Further study is needed to quantify these uncertainties.

Data Availability Statement

Many thanks to the Precipitation Processing System (PPS) team at NASA Goddard Space Flight Center for data processing assistance. All TRMM SLH data can be downloaded at https://pps.gsfc.nasa.gov/; ERA-Interim reanalysis product is available from https://www.ecmwf.int/en/forecasts/datasets/reanalysis-datasets/era-interim.

References

Alexander, M. J., Beres, J. H., & Pfister, L. (2000). Tropical stratospheric gravity wave activity and relationship to clouds. *Journal of Geophysical Research*, *105*(D1722), 22299–22309. https://doi.org/10.1029/2000jd900326

Alexander, M. J., Liu, C., Bacmeister, J., Bramberger, M., Hertzog, A., & Richter, J. H. (2021). Observational validation of parameterized gravity waves from tropical convection in the whole atmosphere community climate model (WACCM). *Journal of Geophysical Research*, *126*, e2020JD033954. https://doi.org/10.1029/2020jd033954

Alexander, M. J., Ortland, D. A., Grimsdell, A. W., & Kim, J. E. (2017). Sensitivity of gravity wave fluxes to interannual variations in tropical convection and zonal wind. *Journal of the Atmospheric Sciences*, *74*, 2701–2716. https://doi.org/10.1175/JAS-D-17-0044.1

Arakawa, A. (2004). The cumulus parameterization problem: Past, present, and future. *Journal of Climate*, *17*, 2493–2525. https://doi.org/10.1175/1520-0442(2004)017<2493:ratcpp>2.0.co;2

Awaka, J., Iguchi, T., & Okamoto, K. (1998). Early results on rain type classification by the Tropical Rainfall Measuring Mission (TRMM) precipitation radar. *Proceedings of 8th URSI Commission F Open Symposium*. (pp. 143–146).

Awaka, J., Kumagai, H., & Iguchi, T. (2009). TRMM PR standard algorithm 2A23 and its performance on bright band detection. *Journal of Meteorological Society of Japan*, *87*, 31–52. https://doi.org/10.2151/jmsj.87a.31

Baldwin, M. P., Gray, L. J., Dunkerton, T. J., Hamilton, K., Haynes, P. H., Randel, W. J., et al. (2001). The quasi-biennial oscillation. *Reviews of Geophysics*, *39*(2), 179–229. https://doi.org/10.1029/1999rg000073

Banta, R. M., Darby, L. S., Fast, J. D., Pinto, J. O., Whiteman, C. D., Shaw, W. J., et al. (2004). Nocturnal low-level jet in a Mountain Basin complex. Part I: Evolution and effects on local flows. *Journal of Applied Meteorology*, *43*, 1348–1365. https://doi.org/10.1175/JAM2142.1

Beres, J., Garcia, R., Boville, B., & Sassi, F. (2005). Implementation of a gravity wave source spectrum parameterization dependent on the properties of convection in the whole atmosphere community climate model (WACCM). *Journal of Geophysical Research*, *110*(D10108). https://doi.org/10.1029/2004JD005504

Beres, J. H., Alexander, M. J., & Holton, J. R. (2004). A method of specifying the gravity wave spectrum above convection based on latent heating properties and background wind. *Journal of the Atmospheric Sciences*, *61*(3), 324–337. https://doi.org/10.1175/1520-0469(2004)061<0324:amostg>2.0.co;2

Bushell, A. C., Butchart, N., Derbyshire, S. H., Jackson, D. R., Shutts, G. J., Vosper, S. B., et al. (2015). Parameterized gravity wave momentum fluxes from sources related to convection and large-scale precipitation processes in a global atmosphere model. *Journal of the Atmospheric Sciences*, *72*(11), 4349–4371. https://doi.org/10.1175/JAS-D-15-0022.1

Butchart, N., Anstey, J. A., Hamilton, K., Osprey, S., McLandress, C., Bushell, A. C., et al. (2018). Overview of experiment design and comparison of models participating in phase 1 of the sparc quasi-biennial oscillation initiative (QBOI). *Geoscientific Model Development*, *11*(3), 1009–1032. https://doi.org/10.5194/gmd-11-1009-2018

Chun, H.-Y., & Baik, J.-J. (2002). An updated parameterization of convectively forced gravity wave drag for use in large-scale models. *Journal of the Atmospheric Sciences*, *59*(5), 1006–1017. https://doi.org/10.1175/1520-0469(2002)059<1006:aupocf>2.0.co;2

Collimore, C. C., Martin, D. W., Hitchman, M. H., Huesmann, A., & Waliser, D. E. (2003). On the relationship between the QBO and tropical deep convection. *Journal of Climate*, *16*, 2552–2568. https://doi.org/10.1175/1520-0442(2003)016<2552:otrbtq>2.0.co;2

Dee, D. P., Uppala, S. M., Simmons, A. J., Berrisford, P., Poli, P., Kobayashi, S., et al. (2011). The ERA-Interim reanalysis: Configuration and performance of the data assimilation system. *Quarterly Journal of the Royal Meteorological Society*, *137*(656), 553–597. https://doi.org/10.1002/qj.828

Emanuel, K. E., Neelin, J. D., & Bretherton, C. S. (1994). On large scale circulations in convecting atmospheres. *Quarterly Journal of the Royal Meteorological Society*, *120*, 1111–1143. https://doi.org/10.1002/qj.49712051902

Ern, M., Trinh, Q. T., Preusse, P., Gille, J. C., Mlynczak, M. G., Russell, J. M., III, et al. (2018). GRACILE: A comprehensive climatology of atmospheric gravity wave parameters based on satellite limb soundings. *Earth System Science Data*, *10*, 857–892. https://doi.org/10.5194/essd-10-857-2018

Funk, A., Schumacher, C., & Awaka, J. (2013). Analysis of rain classification over tropics by Version 7 of TRMM 2A23 algorithm. *Journal of Meteorlogical Society Japan*, *91*, 257–272. https://doi.org/10.2151/jmsj.2013-302

Gettelman, A., Mills, M. J., Kinnison, D. E., Garcia, R. R., Smith, A. K., Marsh, D. R., et al. (2019). The whole atmosphere communicty climate model version 6 (WACCM6). *Journal of Geophysical Research - D: Atmospheres*, *124*(12), 12380–12403. https://doi.org/10.1029/2019JD030943

Giangrande, S. E., Collis, S., Straka, J., Protat, A., Williams, C., & Krueger, S. (2013). A summary of convective-core vertical velocity properties using ARM UHF wind profilers in Oklahoma. *Journal of Applied Meteorlogy and Climatology*, *52*, 2278–2295. https://doi.org/10.1175/JAMC-D-12-0185.1

Giorgetta, M. A., Manzini, E., Roeckner, E., Esch, M., & Bengtsson, L. (2006). Climatology and forcing of the quasi-biennial oscillation in the maecham5 model. *Journal of Climate*, *19*(16), 3882–3901. https://doi.org/10.1175/jcli3830.1

Gray, W. M., & Jacobson, R. W., Jr. (1977). Diurnal variation of deep cumulus convection. *Monthly Weather Review*, *105*(9), 1171–1188. https://doi.org/10.1175/1520-0493(1977)105<1171:dvodcc>2.0.co;2

Gray, W. M., Sheaffer, J. D., & Knaff, J. A. (1992). Hypothesized mechanism for stratospheric QBO influence on ENSO variability. *Geophysical Research Letters*, *19*, 107–110. https://doi.org/10.1029/91gl02950

Hahn, D. G., & Manabe, S. (1975). The role of mountains in the South Asian Monsoon circulation. *Journal of the Atmospheric Sciences*, *32*(8), 1515–1541. https://doi.org/10.1175/1520-0469(1975)032<1515:tromit>2.0.co;2

Hall, T. J., & Vonder Haar, T. H. (1999). The diurnal cycle of west Pacific deep convection and its relation to the spatial and temporal variation of tropical MCSs. *Journal of the Atmospheric Sciences*, *56*, 3401–3415. https://doi.org/10.1175/1520-0469(1999)056<3401:tdcowp>2.0.co;2

Heymsfield, G. M., Tian, L., Heymsfield, A. J., Li, L., & Guimond, S. (2010). Characteristics of deep tropical and subtropical convection from Nadir-viewing high-altitude airborne doppler radar. *Journal of the Atmospheric Sciences*, *67*, 285–308. https://doi.org/10.1175/2009JAS3132.1

Hoffmann, L., & Alexander, M. J. (2009). Retrieval of stratospheric temperatures from AIRS radiance measurements for gravity wave studies. *Journal of Geophysical Research*, *114*. https://doi.org/10.1029/2008JD011241

Hoffmann, L., Xue, X., & Alexander, M. J. (2013). A global view of stratospheric gravity wave hotspots located with atmospheric infrared sounder observations. *Journal of Geophysical Research - D: Atmospheres*, *118*, 416–434. https://doi.org/10.1029/2012jd018658

Houze, R. A., Jr. (1989). Observed structure of mesoscale convective systems and implications for large-scale heating. *Quarterly Journal of Royal Meteorlogical Society*, *115*, 425–461. https://doi.org/10.1002/qj.49711548702

Houze, R. A., Jr, Rasmussen, K. L., Zuluaga, M. D., & Brodzik, S. R. (2015). The variable nature of convection in the tropics and subtropics: A legacy of 16 years of the Tropical Rainfall Measuring Mission (TRMM) satellite. *Reviews of Geophysics*, *53*, 994–1021. https://doi.org/10.1002/2015RG000488

Huffman, G., Adler, R., Morrissey, M., Bolvin, D., Cuttis, S., Joyce, R., et al. (2001). Global precipi- tation at one-degree daily resolution from multisatellite ob- servations. *Journal of Hydrometeorology*, *2*, 36–50. https://doi.org/10.1175/1525-7541(2001)002<0036:gpaodd>2.0.co;2

Iguchi, T., Kozu, T., Kwiatkowski, J., Meneghini, R., Awaka, J., & Okamoto, K. (2009). Uncertainies in the rain profiling algorithm for the TRMM precipitation radar. *Journal of Meteorological Soiety of Japan*, *87*, 11–30. https://doi.org/10.2151/jmsj.87a.1

Iguchi, T., Kozu, T., Meneghini, R., Awaka, J., & Okamoto, K. (2000). Rain-profiling algorithm for the TRMM precipitation radar. *Journal of Applied Meteorology*, *39*, 2038-2052.

Kim, Y.-H., Bushell, A. C., Jackson, D., & Chun, H.-Y. (2013). Impacts of introducing a convective gravity-wave parameterization upon the QBO in the Met office unified model. *Geophysical Research Letters*, *40*, 1873–1877. https://doi.org/10.1002/grl.50353

Kummerow, C., Barnes, W., Kozu, T., Shiue, J., & Simpson, J. (1998). The tropical rainfall measuring mission (TRMM) sensor package. *Journal of Atmospheric and Oceanic Technology*, *15*, 809–817. https://doi.org/10.1175/1520-0426(1998)015<0809:ttrmmt>2.0.co;2

Kwon, Y. C., & Hong, S. (2017). A mass-flux cumulus parameterization scheme across gray-zone resolutions. *Monthly Weather Review*, *145*, 583–598. https://doi.org/10.1175/MWR-D-16-0034.1

Lebsock, M. D., & L'Ecuyer, T. S. (2011). The retrieval of warm rain from CloudSat. *Journal of Geophysical Research*, *116*, D20. https://doi.org/10.1029/2011jd016076

Lin, J. (2007). The double-ITCZ problem in IPCC AR4 coupled GCMs: Ocean–atmosphere feedback analysis. *Journal of Climate*, *20*, 4497–4525. https://doi.org/10.1175/jcli4272.1

Liu, C. (2011). Rainfall contribution from precipitation systems with different sizes, intensities and durations. *Journal of Hydrometeorology*, *12*, 394–412. https://doi.org/10.1175/2010jhm1320.1

Liu, C., Shige, S., Takayabu, Y., & Zipser, E. (2015). Latent heating contribution from precipitation systems with different sizes, depths and intensities in tropics. *Journal of Climate*, *28*, 186–203. https://doi.org/10.1175/jcli-d-14-00370.1

Liu, C., & Zipser, E. J. (2008). Diurnal cycles of precipitation, clouds, and lightning in the triopics from 9 years of TRMM observations. *Geophysical Research Letters*, *35*, L04819. https://doi.org/10.1029/2007GL032437

Liu, C., & Zipser, E. J. (2009). Warm rain in the tropics: Seasonal and regional distribution based on 9 years of TRMM data. *Journal of Climate*, *22*, 767–779. https://doi.org/10.1175/2008JCLI2641.1

Liu, N., Liu, C., Chen, B., & Zipser, E. (2020). What are the favorable large-scale environments for the most intense thunderstorms on Earth? *Journal of the Atmospheric Sciences*, *77*, 1583–1612. https://doi.org/10.1175/jas-d-19-0235.1

Liu, N., Liu, C., & Lavigne, T. (2019). The variation of the intensity, height and size of precipitation systems along with EL Nino-Southern Oscillation in the tropics and subtropics. *Journal of Climate*, *32*, 4281–4297. https://doi.org/10.1175/JCLI-D-18-0766.1

Miller, S. T. K., Keim, B. D., Talbot, R. W., & Mao, H. (2003). Sea breeze: Structure, forecasting, and impacts. *Reviews of Geophyics*, *41*, 1011. https://doi.org/10.1029/2003RG000124

Nesbitt, S. W., & Zipser, E. J. (2003). The diurnal cycle of rainfall and convective intensity according to three years of TRMM measurements. *Journal of Climate*, *16*, 1456–1475. https://doi.org/10.1175/1520-0442-16.10.1456

Parker, D. J., Burton, R. R., Diongue-Niang, A., Ellis, R. J., Felton, M., Taylor, C. M., et al. (2005). The diurnal cycle of the West African monsoon circulation. *Quarterly Journal of the Royal Meteorological Society*, *131*, 2839–2860. https://doi.org/10.1256/qj.04.52

Power, S. B., & Smith, I. N. (2007). Weakening of the Walker Circulation and apparent dominance of El Niño both reach record levels, but has ENSO really changed? *Geophysical Research Letters*, *34*, L18702. https://doi.org/10.1029/2007GL030854

Richter, J. H., Sassi, F., & Garcia, R. R. (2010). Toward a physically based gravity wave source parameterization in a general circulation model. *Journal of the Atmospheric Sciences*, *67*(1), 136–156. https://doi.org/10.1175/2009JAS3112.1

Rossow, W. B., & Schiffer, R. A. (1999). Advances in understanding clouds from ISCCP. *Bulletin of the American Meteorological Society*, *80*, 2261–2287. https://doi.org/10.1175/1520-0477(1999)080<2261:aiucfi>2.0.co;2

Schumacher, C., & Houze, R. A. (2003). Stratiform rain in the tropics as seen by the TRMM precipitation radar. *Journal of Climate*, *16*, 1739–1756. https://doi.org/10.1175/1520-0442(2003)016<1739:sritta>2.0.co;2

Schumacher, C., Houze, R. A., Jr, & Kraucunas, I. (2004). The tropical dynamical response to latent heating estimates derived from the TRMM precipitation radar. *Journal of the Atmospheric Sciences*, *61*, 1341–1358. https://doi.org/10.1175/1520-0469(2004)061<1341:ttdrtl>2.0.co;2

Shige, S., Takayabu, Y. N., Kinda, S., Tao, W.-K., Zeng, X., et al. (2009). Spectral retrieval of latent heating profiles from TRMM PR data. Part IV: Comparisons of lookup tables from two- and three-dimensional cloud-resolving model simulations. *Journal of Climate*, *22*, 5577–5594. https://doi.org/10.1175/2009jcli2919.1

Shige, S., Takayabu, Y. N., Tao, W.-L., & Johnson, D. E. (2004). Spectral retrieval of latent heating profiles from TRMM PR data. Part I: Development of a model-based algorithm. *Journal of Applied Meteorology*, *43*, 1095–1113. https://doi.org/10.1175/1520-0450(2004)043<1095:srolhp>2.0.co;2

Takayabu, Y. N., Shige, S., Tao, W.-K., & Hirota, N. (2010). Shallow and deep latent heating modes over tropical oceans observed with TRMM PR spectral latent heating data. *Journal of Climate*, *23*, 2030–2046. https://doi.org/10.1175/2009jcli3110.1

Tao, W.-K., Smith, E. A., Adler, R. F., Haddad, Z. S., Hou, A. Y., Iguchi, T., et al. (2006). Retrieval of latent heating from TRMM measurements. *Bulletin of the American Meteorological Society*, *87*, 1555–1572. https://doi.org/10.1175/bams-87-11-1555

Tao, W.-K., Takayabu, Y. N., Lang, S., Shige, S., Olson, W., Hou, A., et al. (2016). TRMM latent heating retrieval: Applications and comparisons with field campaigns and large-scale analyses. *Meteorological Monographs*, *56*, 2–12. https://doi.org/10.1175/amsmonographs-d-15-0013.1

Weisman, M. L., & Klemp, J. B. (1982). The dependence of numerically simulated convective storms on vertical wind shear and buoyancy. *Monthly Weather Review*, *110*, 504–520. https://doi.org/10.1175/1520-0493(1982)110<0504:tdonsc>2.0.co;2

Weisman, M. L., & Rotunno, R. (2000). The use of vertical wind shear versus helicity in interpreting supercell dynamics. *Journal of the Atmospheric Sciences*, *57*, 1452–1472. https://doi.org/10.1175/1520-0469(2000)057<1452:tuovws>2.0.co;2

Wolter, K., & Timlin, M. S. (2011). El Niño/Southern Oscillation behaviour since 1871 as diagnosed in an extended multivariate ENSO index (MEI.ext). *International Journal of Climatology*, *31*, 14. https://doi.org/10.1002/joc.2336

Zhang, G., Song, X., & Wang, Y. (2019). The double ITCZ syndrome in GCMs: A coupled feedback problem among convection, clouds, atmospheric and ocean circulations. *Atmospheric Research*, *229*, 255–268. https://doi.org/10.1016/j.atmosres.2019.06.023

Zipser, E. J., Liu, C., Cecil, D., Nesbitt, S. W., & Yorty, S. (2006). where are the most intense thunderstorms on Earth? *Bulletin of American Meteorological Research*, *87*, 1057–1072. https://doi.org/10.1175/bams-87-8-1057